Available online at www.sciencedirect.com
ScienceDirect
Journal of Power Sources 184 (2008) 682–690
JOURNAL OF POWER SOURCES
www.elsevier.com/locate/jpowsour

Fabrication and electrochemical characterization of cobalt-based layered double hydroxide nanosheet thin-film electrodes

Yi Wang, Wensheng Yang *, Chen Chen, David G. Evans

State Key Laboratory of Chemical Resource Engineering, Beijing University of Chemical Technology, Beijing 100029, China

Received 23 November 2007; received in revised form 16 January 2008; accepted 3 February 2008
Available online 17 February 2008

Abstract

A continuous cobalt-based layered double hydroxide (LDH) nanosheet thin-film electrode has been fabricated by drying a nearly transparent colloidal solution of cobalt-based LDH nanosheets on an indium tin oxide (ITO)-coated glass plate substrate. The effects of varying the Al content, the film thickness, and the heating temperature on the electrochemical properties of the as-deposited thin-film electrode have been investigated. A thin-film electrode with a Co/Al molar ratio of 3:1, which has a large specific capacitance of 2500 F cm^{-3} (833 F g^{-1}) and a good high-rate capability, shows the best performance when used as an electrode in thin-film supercapacitors (TFSCs). As the thickness of the thin film was increased from 100 to 500 nm, the specific capacitance of the thin-film electrode remained essentially unchanged, which is due to the porous microstructure generated in the original electrochemical process and the low internal resistance of the thin-film electrode. The specific capacitance of the thin-film electrode showed no observable change after heating at 160 °C, but decreased on further heating to 200 °C, indicating that the electrochemically active Co sites inside the thin-film nanosheet electrode are already essentially fully exposed in the as-prepared material and hence cannot be further exposed through heating. Such a thin-film electrode made up of nanosheets may be a potential economical alternative electrode for use in TFSCs.

Keywords: Supercapacitor; Thin-film electrode; Nanosheets; Co–Al layered double hydroxides

1. Introduction

Interest in micro-scale power sources, such as thin-film batteries (TFBs) and thin-film supercapacitors (TFSCs), has risen in recent years because of their use as power sources in microelectronic mechanical systems (MEMs) and nanoelectronic mechanical systems (NEMs) [1–11]. TFBs are suitable for use in most of these devices as a result of their high energy density, rechargeability, and safety in operation. However, their poor ability to deliver high power over limited time intervals limits the applications of TFBs in some special fields such as the startup of some MEMs or NEMs, which require a large burst of power to be delivered in a very short time. To meet this particular demand, the fabrication of high-quality TFSCs with high power density and long cycle life has received considerable attention in recent years [5–8].

Supercapacitors (also called electrochemical capacitors) that can fill the gap between batteries and conventional dielectric capacitors have considerable potential for use in high power applications [12,13]. Supercapacitors may be distinguished on the basis of several criteria such as the electrode material utilized, the electrolyte, or the cell design. With respect to electrode material there are three main categories: carbon, (hydrous) metal oxides, and conducting polymers [14]. To date, conducting noble metal oxides like RuO_2 or IrO_2 are the favored electrode materials for supercapacitors [15–19]. Although RuO_2 gives high specific capacitance (as high as 1300 F g^{-1} [17,18]), it has the disadvantages of high cost and toxic nature, which limit its commercial applications. Therefore other transition metal oxides, such as amorphous hydrous cobalt–nickel oxides [20], MnO_2 [21], NiO [22], Co_3O_4 [23], and Fe_3O_4 [24] have been examined as inexpensive alternatives to RuO_2. In addition to good supercapacitor behavior, metal oxides also have the advantage that they can be readily made into thin films. For example, RuO_2 and Co_3O_4 thin-film electrodes have been fabricated for use as the electrodes for TFSCs by a radio frequency (rf) sputtering

* Corresponding author. Tel.: +86 10 64435271; fax: +86 10 64425385.
E-mail address: yangws@mail.buct.edu.cn (W. Yang).

0378-7753/$ – see front matter © 2008 Elsevier B.V. All rights reserved.
doi:10.1016/j.jpowsour.2008.02.017

method [5,6]. However, sputtering [2,4–6,10] and most of the other techniques for making thin-film electrodes, such as pulse laser deposition (PLD) [11], require high energy, high material consumption, and complicated equipment. Furthermore, using such processes it is difficult to fabricate hydrous metal oxides, which usually have better supercapacitor behavior than crystalline metal oxides [15,16]. Thus, an alternative route to synthesize hydrous metal oxide thin-film electrodes which is less energy intensive, more economical, and requires simpler apparatus is highly desirable.

We have recently suggested a simple strategy to fabricate a Co/Al LDH nanosheet thin-film electrode with good supercapacitor behavior for use in TFSCs [25]. In this work, our aim is to tailor the supercapacitor behavior of the cobalt-based LDH nanosheet (Co/Al-LDH NS) thin-film electrodes prepared by this procedure. The relationship between the chemical composition and the electrochemical properties of the thin films has been investigated in detail. The effects of varying the thickness and the temperature of formation of the thin film on the electrochemical behavior have also been studied.

2. Experimental

2.1. Synthesis of nitrate anion-intercalated cobalt-based LDHs with varying Al content

Nitrate anion-intercalated cobalt-based LDHs ($Co_{1-x}Al_x$-LDHs) with varying Al content x were synthesized by a method involving separate nucleation and aging steps (SNAS) [26,27]. Water used in all preparations was deionized with a conductance below 10^{-6} S cm^{-1}. Details for a typical synthesis are as follows. Solution A: $Co(NO_3)_2{\cdot}6H_2O$ and $Al(NO_3)_3{\cdot}9H_2O$ with a Co/Al molar ratio of 2:1 (i.e. $x = 0.33$) were dissolved in deionized water (150 mL) to give a solution with a total metal ion concentration of 1.0 mol L^{-1}. Solution B: NaOH was dissolved in deionized water (150 mL). The concentration of the base was related to the concentration of metal ions in solution A as follows: $[OH^-] = 1.9\{[Co^{2+}] + [Al^{3+}]\}$. Solutions A and B were added simultaneously to a colloid mill [26,27] with rotor speed set at 3000 rpm and mixed for 2 min. The resulting slurry was transferred from the colloid mill to a flask (500 mL) and aged at 40 °C for 6 h. The precipitate was centrifuged and washed thoroughly with deionized water until the pH of the washings was <8. The resulting solid was dried at 80 °C for 24 h. Nitrate anion-intercalated $Co_{1-x}Al_x$-LDHs with Co/Al ratios of 3:1 and 4:1 ($x = 0.25$ and 0.20, respectively) were synthesized using the same procedure.

2.2. Synthesis of nitrate anion-intercalated cobalt-based LDHs without Al

An NaOH solution (0.5 mol L^{-1}) was added to a solution of $Co(NO_3)_2{\cdot}6H_2O$ (1.0 mol L^{-1}) and $NaNO_3$ (5.0 mol L^{-1}) under a nitrogen atmosphere. The Co^{2+} was partially oxidized to Co^{3+} by subsequent dropwise addition of 2 mL of H_2O_2 solution (10.0 mol L^{-1}). The reaction mixture was subsequently heated at 40 °C for 6 h, washed several times with hot deionized water until the pH of the washings was <8, centrifuged, and the resulting solid finally dried at 80 °C for 24 h.

2.3. Delamination of nitrate anion-intercalated cobalt-based LDHs with different Al contents

Samples (0.1 g) of the as-prepared powdery nitrate anion-intercalated $Co_{1-x}Al_x$-LDHs with $x = 0$, 0.20, 0.25 or 0.33 were mixed with formamide (100 mL). The mixture was agitated vigorously at 85 °C for 2 h. To remove the unexfoliated particles, the resulting pink, transparent colloidal suspension was further treated by centrifugation at 10,000 rpm for 20 min. The resulting colloidal suspension was very stable, and no sediment was observed upon long-term standing.

2.4. Fabrication of cobalt-based LDH nanosheet thin-film electrodes with varying Al content

Thin-film electrodes with $x = 0$, 0.20, 0.25 or 0.33 were prepared by dropping 500 μL of the colloidal formamide solution of the corresponding exfoliated LDH nanosheets (1 g L^{-1}) onto ITO substrates (resistance ≤20 Ω cm^{-2}) with a flat ($R_a = 0.2$ nm) and negatively charged surface, which had been previously cleaned by sonication in acetone, ethanol, and doubly distilled water, and then dried at 80 °C for 24 h, to form a film with an area of 4.0 cm^2. The $Co_{0.80}Al_{0.20}$-LDH NS thin film was further heated at 160 and 200 °C in air for 2 h.

2.5. Characterization

Powder X-ray diffraction (XRD) patterns of the samples were collected using a Shimadzu XRD6000 diffractometer under the following conditions: 40 kV, 30 mA, graphite-filtered Cu Kα radiation ($\lambda = 0.15418$ nm). Room temperature Fourier transform infrared (FT-IR) spectra were recorded in the range 4000–400 cm^{-1} with 2 cm^{-1} resolution on a Bruker Vector-22 Fourier transform spectrometer using the KBr pellet technique (1 mg of sample in 100 mg of KBr). Elemental analyses of the as-prepared LDH particles and nanosheets were performed with a Shimadzu ICP-7500 instrument. A Hitachi S-4700 field emission scanning electron microscope (FE-SEM) and an Oxford Instruments Isis300 energy dispersive X-ray spectrometer (EDX) were employed to observe the morphologies of the samples and analyze the chemical compositions of the as-deposited thin-film electrodes. The accelerating voltage was 20 kV.

2.6. Electrochemical investigations

The electrochemical characterization of the as-prepared $Co_{1-x}Al_x$-LDH NS thin-film electrodes with different Al content x were investigated using cyclic voltammetry (CV) and galvanostatic charge–discharge experiments. Beaker-type half-cells were used to characterize the electrochemical properties of the as-prepared thin-film electrode coatings on the ITO substrate. The electrochemical cell consisted of a thin-film electrode with geometric surface area of 4 cm^2 as working electrode,

a platinum wire as counter electrode, an Hg/HgO electrode as reference electrode, and a 6 mol L^{-1} KOH aqueous solution as electrolyte. Cyclic voltammograms (CVs) were recorded with a scan rate of 10 or 100 mV s^{-1} in the range 0.00–0.60 V (vs. Hg/HgO) using a Zahner IM6e electrochemical workstation. The working electrode was scanned between 0.00 and 0.60 V (vs. Hg/HgO) at a scan rate of 100 mV s^{-1} 20 times prior to the galvanostatic charge–discharge experiment and the galvanostatic charge–discharge was evaluated with an Arbin MSTAT4 + multichannel galvanostat/potentiostat in the potential range 0.00–0.50 or 0.55 V (vs. Hg/HgO). All measurements were carried out at room temperature.

The volumetric specific capacitance (C_v) was measured by galvanostatic charge–discharge and calculated using the formula $I \times \Delta t/(S \times L \times \Delta V)$, where I is the discharge current, Δt is the total discharge time, S is the geometric surface area of the electrode, L is the thickness of the LDH NS thin film, and ΔV is the potential drop during discharging. The mass specific capacitance (C_m) was calculated from C_v/TD, where TD is the true density of the LDH NS thin-film electrode. According to the literature [28], the value of TD is about 3.00 g cm^{-3}. Considering that two-electron redox reactions (from Co^{2+} to Co^{4+}) are assumed to take place throughout the bulk material, the theoretical specific capacitance, C_t, was estimated by $n \times F/(M \times \Delta V)$ [29], where n (= 2) is the number of moles of charge transferred per mole of $Co_{1-x}Al_x$-LDHs, F is Faraday's constant, M is the molar mass of the $Co_{1-x}Al_x$-LDHs, and ΔV is the potential drop during discharging. The utilization of Co is calculated on the basis of C_m/C_t.

3. Results and discussion

3.1. Characterization of the cobalt-based LDH nanosheet thin-film electrodes with varying Al content

The powder XRD patterns of nitrate anion-intercalated $Co_{1-x}Al_x$-LDHs prepared using mixtures with different Al content x are shown in Fig. 1. In each case, the XRD pattern exhibits

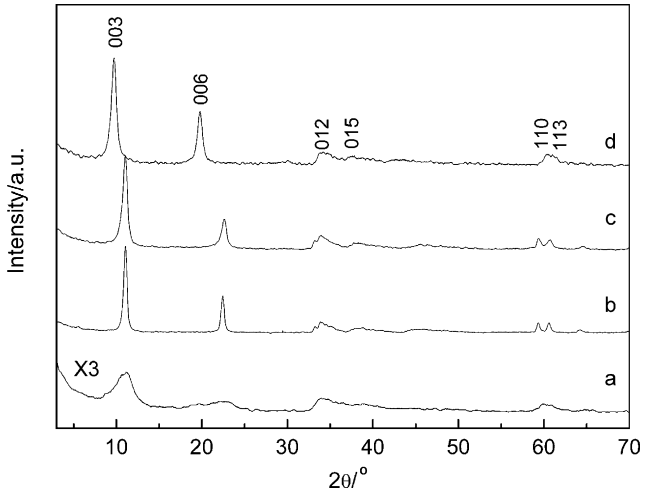

Fig. 1. Powder XRD patterns of nitrate anion-intercalated $Co_{1-x}Al_x$-LDHs with different Al content x (a: $x = 0$; b: $x = 0.20$; c: $x = 0.25$; d: $x = 0.33$).

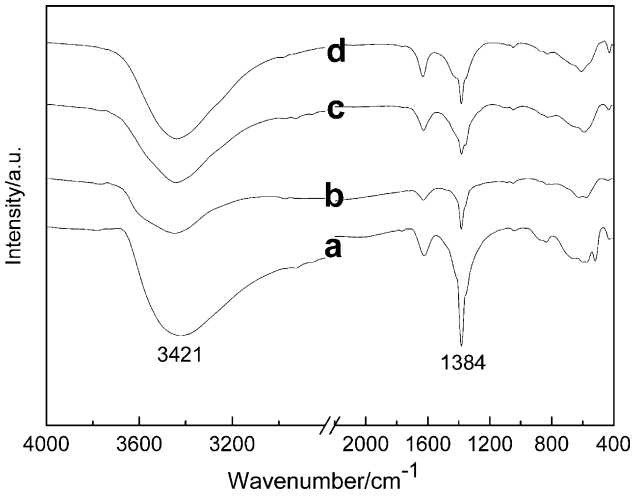

Fig. 2. FT-IR spectra of $Co_{1-x}Al_x$-LDHs with different Al content x (a: $x = 0$; b: $x = 0.20$; c: $x = 0.25$; d: $x = 0.33$).

the characteristic reflections of LDHs with a series of (0 0 l) peaks appearing as narrow symmetric lines at low angle, corresponding to the basal spacing and higher order reflections. No other crystalline phase was present. FT-IR spectra (Fig. 2) of the $Co_{1-x}Al_x$-LDHs with different Al content x showed absorption bands corresponding to the intercalated nitrate anions, which give a very intense absorption at 1383 cm^{-1}. The characteristic peak of carbonate anions centered at 1356 cm^{-1} was not observed, suggesting that the amount of co-intercalated carbonate anions is minimal. A broad absorption peak centered at ca. 3421 cm^{-1} can be attributed to the stretching mode of hydrogen-bonded hydroxyl groups from both the hydroxide layers and interlayer water.

The $Co_{1-x}Al_x$-LDH NS with different Al content x were obtained by exfoliating the as-prepared $Co_{1-x}Al_x$-LDH precursors into single layers in formamide solution [25]. In each case, a stable transparent pink colloidal solution was obtained, which is indicative of the fact that the charge density of the LDH layers has no significant effect on the delamination process.

The $Co_{1-x}Al_x$-LDH NS with different Al content x were used as building blocks to fabricate thin-film electrodes. The chemical compositions of the as-deposited thin-film electrodes and their precursors are given in Table 1. The Co/Al molar ratio in each thin-film electrode is close to that in the corresponding precursor nanoparticles and nanosheets. To characterize the surface morphologies of the as-deposited thin-film electrodes with

Table 1
Elemental analysis date (obtained by ICP and EDX) for the nitrate anion-intercalated $Co_{1-x}Al_x$-LDHs with different Al content x

Co/Al molar ratio in synthesis mixture	Co/Al molar ratio		
	In nanoparticles[a]	In nanosheets[a]	In thin films[b]
2.00	1.85	1.85	1.99
3.00	2.78	2.73	2.73
4.00	4.56	4.48	4.07

[a] Obtained by ICP.
[b] Obtained by EDX.

different Al contents, FE-SEM was employed and the results are shown in Fig. 3. It can be observed that for all the thin-film electrodes, there is a continuous microstructure with edges of the nanosheets only rarely being visible; this is a result of the prevalence of face-to-face interactions and edge-to-edge interactions between the neighboring individual LDH nanosheets [30,31]. Moreover, the surface roughness of the thin-film electrode without Al is higher than that of those containing Al. This may be due to the fact that the particle size distributions of the $Co_{1-x}Al_x$-LDH precursors containing Al ($x>0$), which were synthesized by the SNAS method, are narrower than that for the LDHs without Al ($x=0$), which was synthesized by a conventional coprecipitation method [26]. In addition, the structural stability of $Co_{1-x}Al_x$-LDHs increases with the extent of isomor-

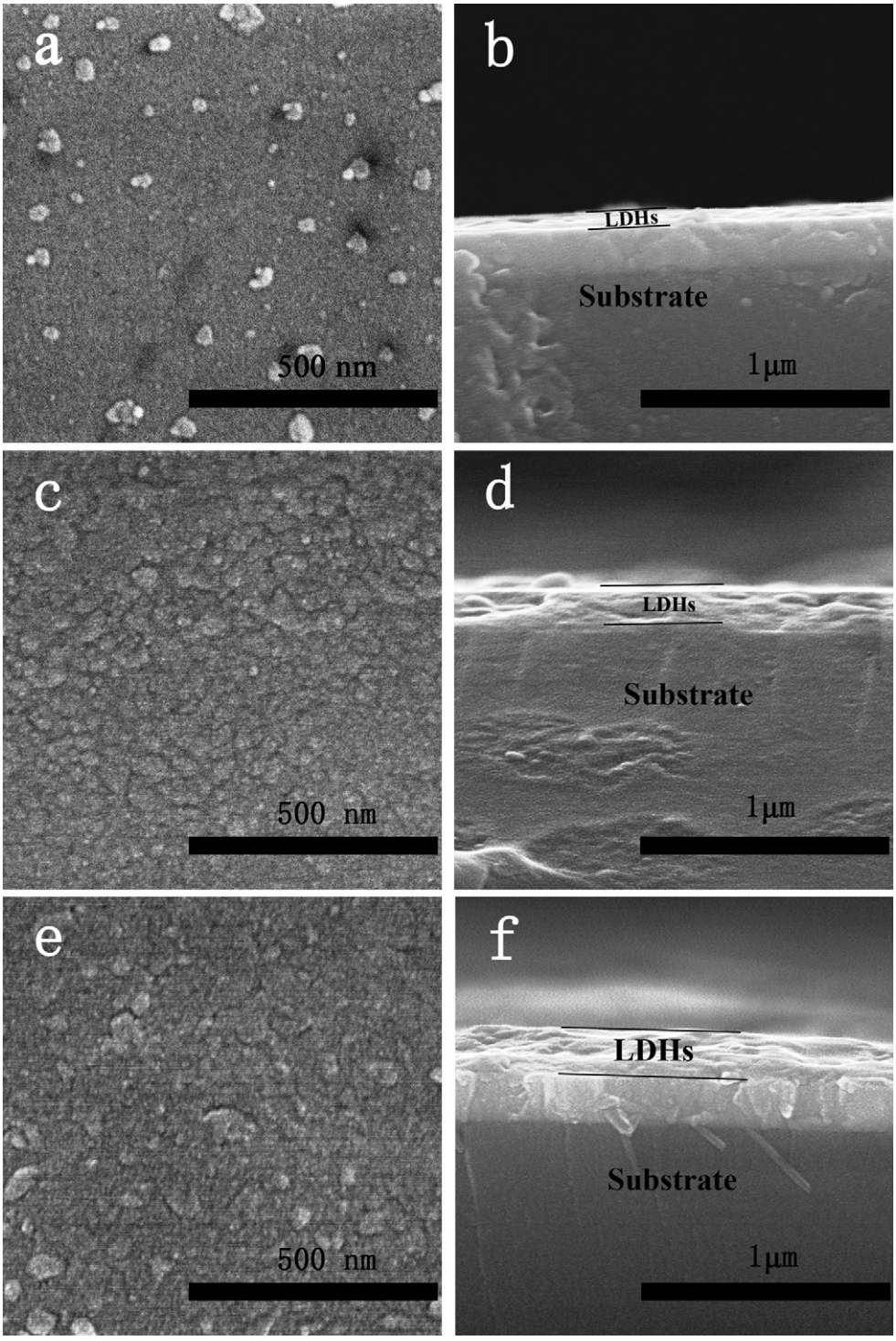

Fig. 3. FE-SEM images in top view (a, c, e, g) and cross-sectional view (b, d, f, h) of the $Co_{1-x}Al_x$-LDH NS thin-film electrodes with different Al content x (a: $x=0$; b: $x=0.20$; c: $x=0.25$; d: $x=0.33$).

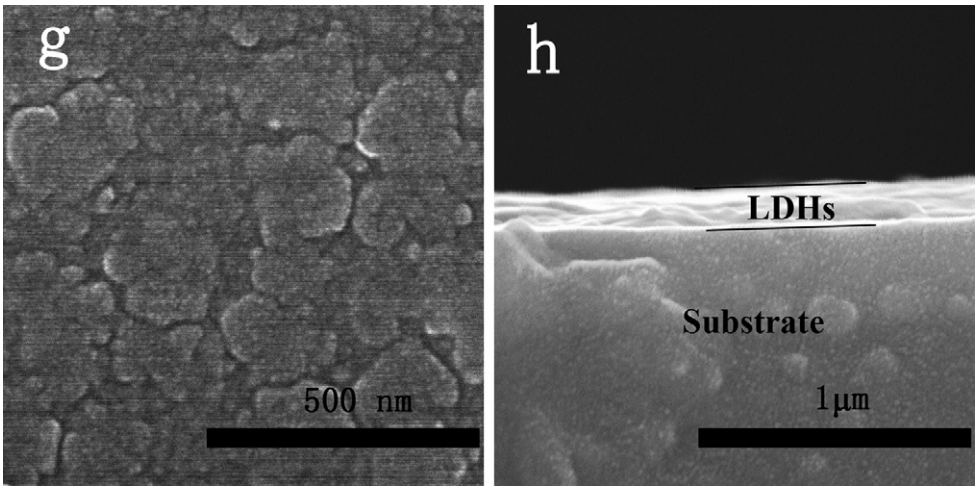

Fig. 3. (*Continued*).

phous substitution of Co^{2+} by Al^{3+} (i.e. as x increases) and the $Co_{1-x}Al_x$-LDH NS with higher Al content are therefore more stable during the delamination process. This may be another possible reason for the minor variation with x of the morphology of the $Co_{1-x}Al_x$-LDH NS thin-film electrodes with $x>0$.

3.2. The effect of varying the Al content x on the electrochemical properties

CV and charge–discharge measurements were employed in order to investigate the effect of varying the Al content on the electrochemical behavior. The CVs of the $Co_{1-x}Al_x$-LDH NS thin-film electrodes with different Al contents at a sweep rate of 10 mV s^{-1} are shown in Fig. 4. It can be observed that the shape of the CVs shows a typical behavior of Co oxides [29], indicating that the Co is the electroactive component and the Al is non-electroactive during the charge–discharge process. However, although the Al is not active, the partial isomorphous substitution of Co^{2+} with Al^{3+} leads to a shift in the oxygen evolution overpotential to a more positive value, which helps to improve the charge efficiency of the electrode.

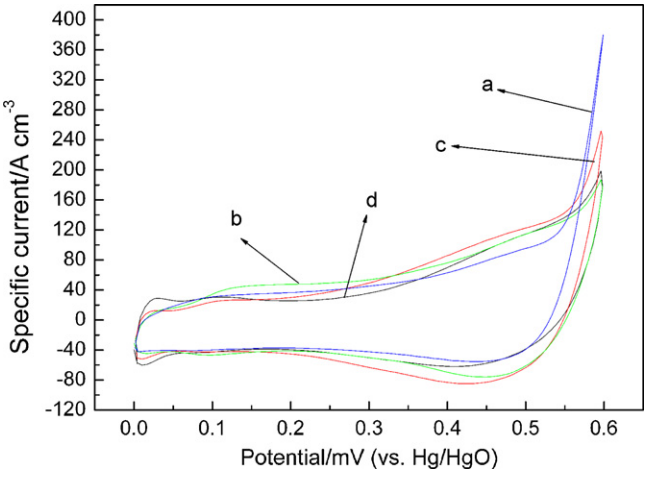

Fig. 4. Cyclic voltammograms of the $Co_{1-x}Al_x$-LDH NS thin-film electrodes with different Al content x at a sweep rate of 10 mV s^{-1} (a: $x=0$; b: $x=0.20$; c: $x=0.25$; d: $x=0.33$).

Constant current charge–discharge profiles measured at different specific currents for the $Co_{1-x}Al_x$-LDH NS thin-film electrodes with different Al contents are shown in Fig. 5. The specific capacitance as a function of the discharge rate is illustrated in Fig. 6. As shown there, the high-rate capability of the thin-film electrode increases with decreasing Al content x. This is as expected, since Co is an electroactive material whilst Al is a non-electroactive material. Increasing the Co content decreases the internal resistance, which enhances the high-rate capability. Since Al has no electrochemical activity, it is to be expected that the theoretical specific capacitance of the thin-film electrode shows a decrease with increasing Al content x (as shown in Table 2). In practice however, the thin-film electrode incorporating Al has a higher specific capacitance than that without Al. This is because although the Al is not electroactive, the partial isomorphous substitution of Co^{2+} by Al^{3+} favors the retention of the original layered structure during the redox reaction. Thus, in the $Co_{1-x}Al_x$-LDH NS thin-film electrodes containing Al ($x>0$), Co can be oxidized to a higher oxidation state in a multi-electron process. The oxidation reaction occurs topochemically in the layers, forming CoO_2, which can enhance the discharge specific capacitance of the thin-film electrode [32,33]. The utilization of Co has also been calculated and the results are presented in Table 2. The Co utilization increases with increasing Al content x. As mentioned above, in view of its low cost, high specific capacitance, high utilization of Co, and good high-rate capability

Table 2
The theoretical specific capacitance (C_t), the experimental specific capacitance (C_m) with a discharge rate of 10 C, and the Co utilization (U) of the $Co_{1-x}Al_x$-LDH NS thin-film electrodes with different Al content x

Al content x	C_t (F g^{-1})	C_m (F g^{-1})	U (%)
0	2830	607	21
0.20	2580	800	32
0.25	2300	833	36
0.33	2050	827	38

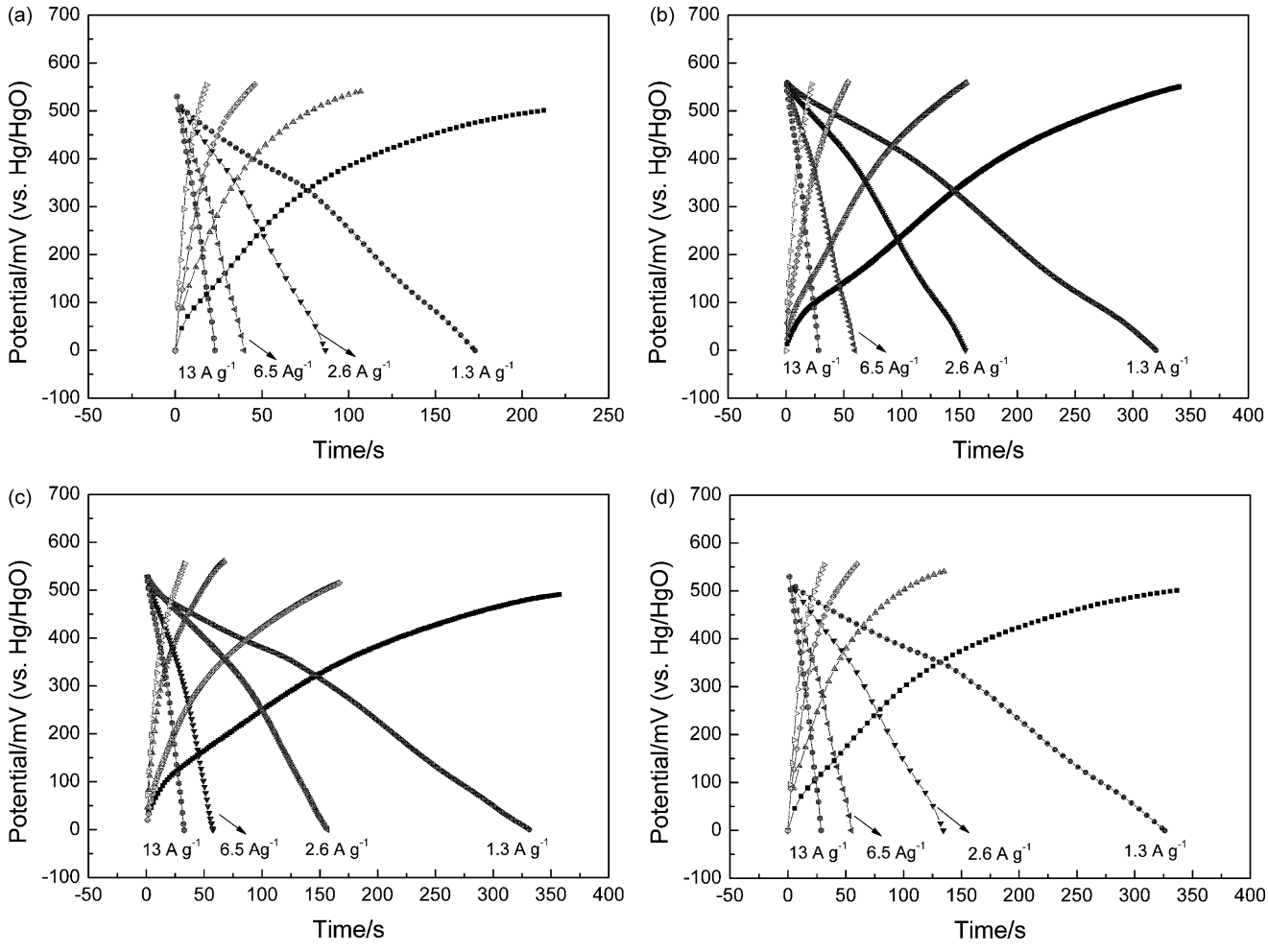

Fig. 5. Charge–discharge curves of the $Co_{1-x}Al_x$-LDH NS thin-film electrodes with different Al content x at different specific discharge currents (a: $x = 0$; b: $x = 0.20$; c: $x = 0.25$; d: $x = 0.33$).

we think that the thin-film electrode with $x = 0.25$ is eminently suitable for use as the electrode in TFSCs.

It should be noted that the packed structure could present an obstacle to diffusion of OH^- ions, which would decrease the utilization of Co. However, the cobalt utilization of the thin-film electrode with $x = 0.25$ was 36%, higher than the value of 17% reported in the literature for cobalt oxides [34]. This suggested to us that the microstructure undergoes a change during the redox reaction. FE-SEM was employed to test this hypothesis. As shown in Fig. 7, the surface morphology of the thin-film electrode with $x = 0.25$ became more porous during the original electrochemical process (20 cycles) and remained essentially unchanged during the following redox reaction. The porous microstructure generated will facilitate the diffusion of OH^- ions and hence increase the utilization of Co. Although the microstructure undergoes a change during the redox reaction, the thin-film electrode retains a good electrochemical stability (as shown in Fig. 8), which can be attributed to its continuous microstructure. Furthermore, it can be observed in Fig. 8 that the thin-film electrode with $x = 0.25$ retained 95% of its reversible specific capacitance up to 2000 cycles, whereas for the thin-film electrode without Al less than 90% of the reversible specific capacitance was retained after the same number of cycles. These results further confirm that the presence of Al in the layers, which can help to prevent the agglomeration of electroactive Co element, is another key factor in improving the electrochemical stability during the charge–discharge processes.

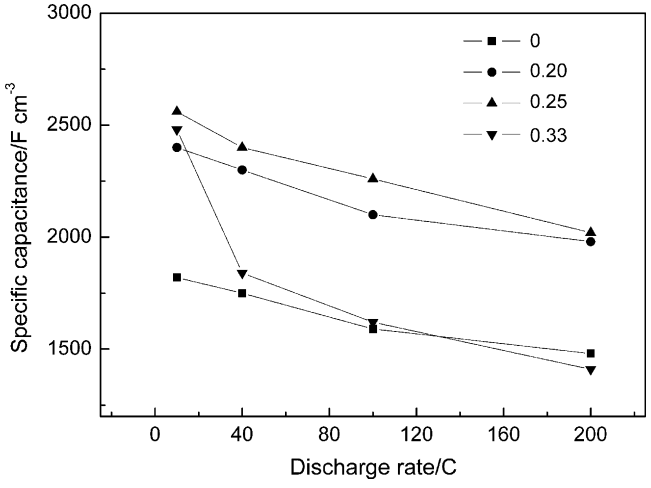

Fig. 6. The specific capacitance of the $Co_{1-x}Al_x$-LDH NS thin-film electrodes with different Al content x as a function of the discharge rate.

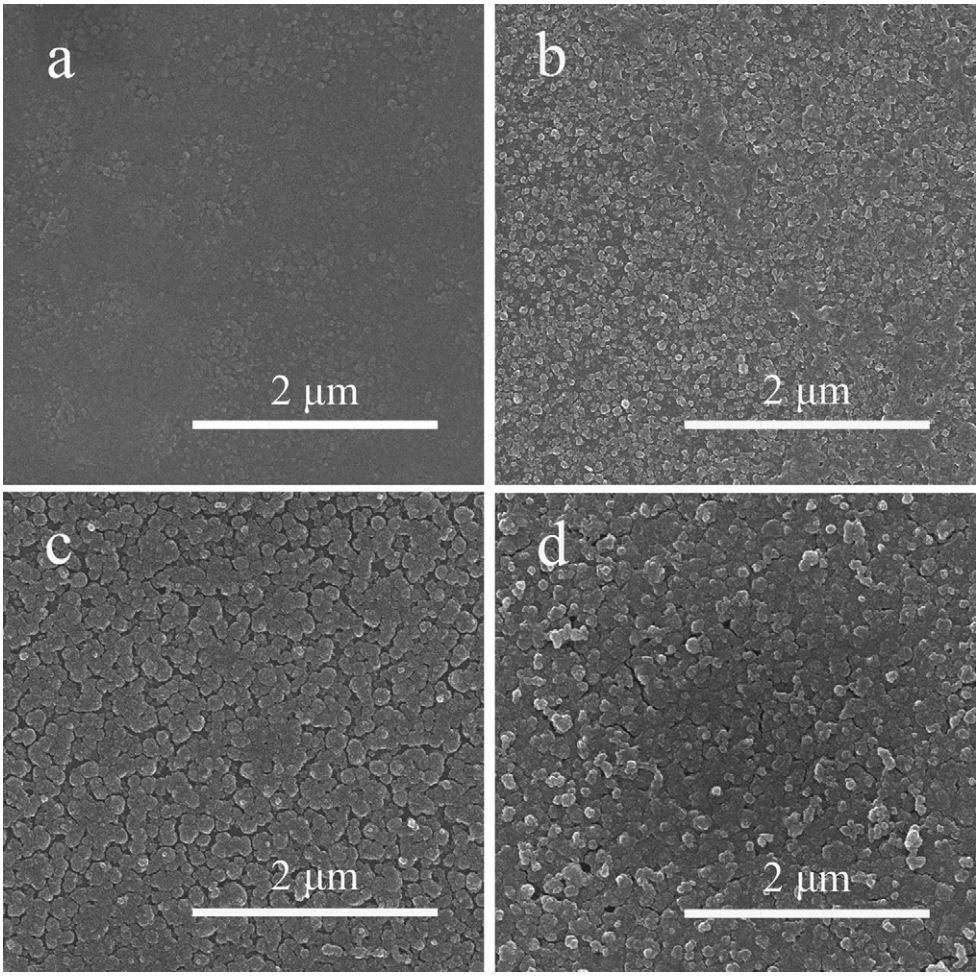

Fig. 7. FE-SEM images of the $Co_{0.75}Al_{0.25}$-LDH NS thin-film electrode after different numbers of cycles in a CV test at a sweep rate of 100 mV s^{-1} (a: as-deposited; b: 1 cycle; c: 20 cycles; d: 500 cycles).

3.3. The effect of the film thickness on the electrochemical properties of the thin-film electrode

The thickness of the thin film, which can affect the electrochemical behavior, can easily be adjusted by increasing the deposition times. The specific capacitance of the $Co_{0.80}Al_{0.20}$-LDH NS thin-film electrode as a function of the film thickness is shown in Fig. 9. The diffusion barrier for both OH^- ions and cations should increase sharply with increasing film thickness. However, the specific capacitance of the thin-film electrode

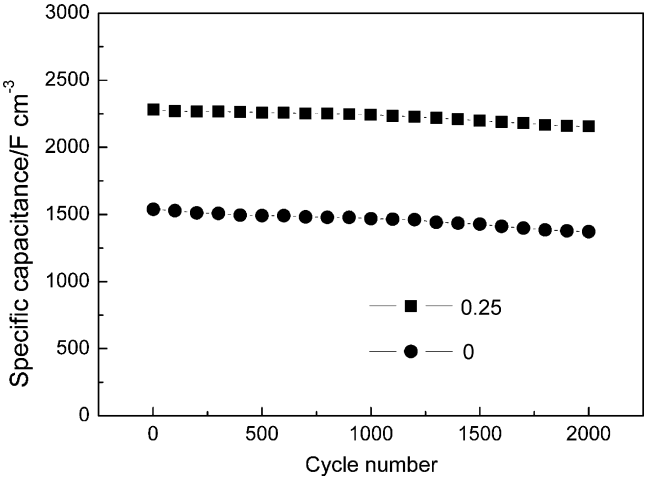

Fig. 8. The specific capacitance of the $Co_{1-x}Al_x$-LDH NS thin-film electrodes with $x = 0$ and 0.25 as a function of the cycle number at a discharge rate of 90 C.

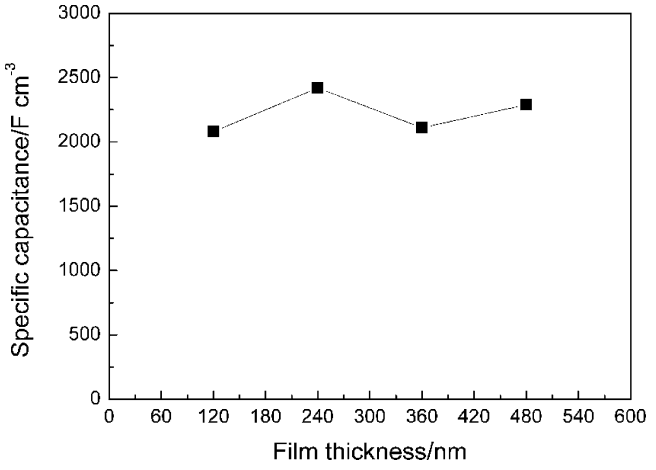

Fig. 9. The specific capacitance of the $Co_{0.80}Al_{0.20}$-LDH NS thin-film electrode as a function of the film thickness.

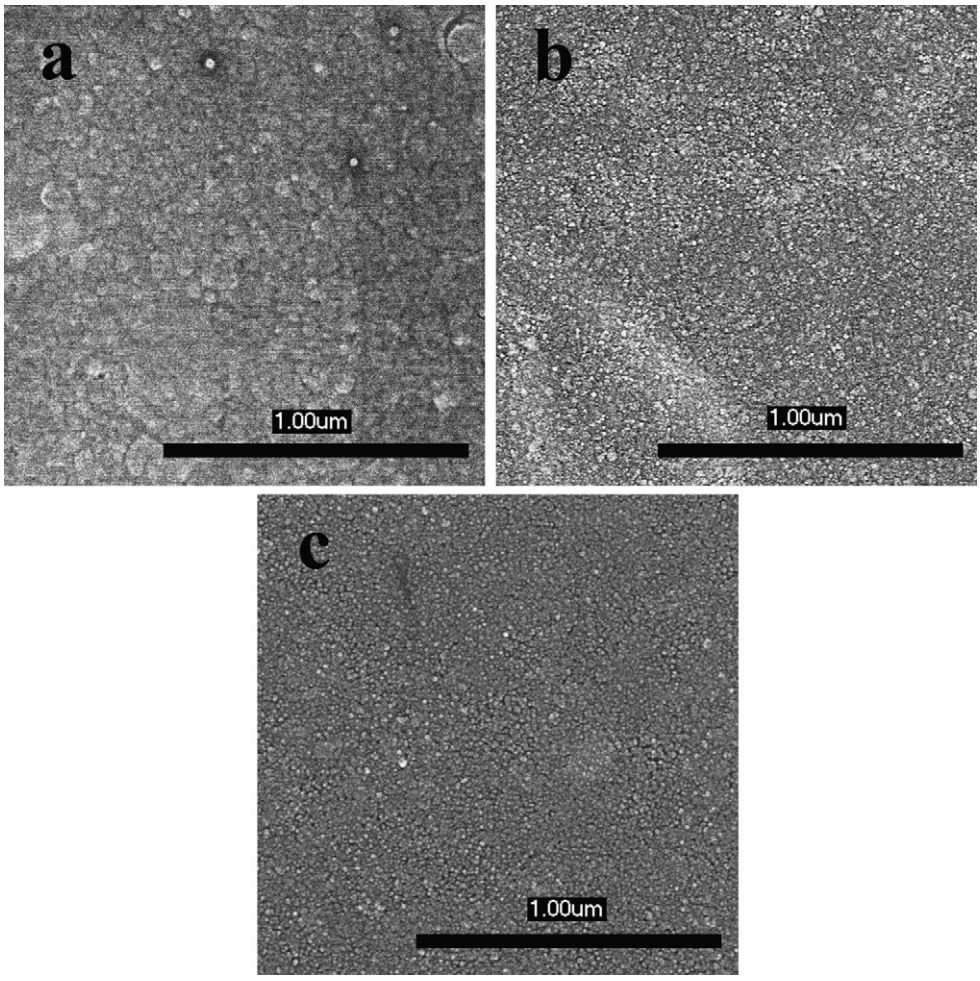

Fig. 10. FE-SEM images of the $Co_{0.80}Al_{0.20}$-LDH NS thin-film electrode heated at different temperatures (a: 80 °C; b: 160 °C; c: 200 °C).

showed almost no change as the thickness increased from 100 to 500 nm. Thus, we think that the porous microstructure generated during the original charge–discharge process resulted in more electrochemically active Co sites being in direct contact with the electrolyte. Moreover, the continuous microstructure of the thin-film electrode can help to decrease the internal resistance, which leads to an improvement in the high-rate capability.

3.4. The effect of heating temperature on the electrochemical properties of the thin-film electrode

The effect of varying the heating temperature on the electrochemical properties of the $Co_{0.80}Al_{0.20}$-LDH NS thin-film electrode was also studied in detail. The FE-SEM images of the surface morphologies of the thin-film electrodes heated at different temperatures are shown in Fig. 10. It can be observed that the surface morphology of the thin-film electrode becomes rougher with increasing heating temperature, which can be attributed to the decomposition of the $Co_{0.80}Al_{0.20}$-LDH NS thin film within this temperature range. The variation in specific capacitance as a function of the heating temperature is illustrated in Fig. 11. It can be seen that the specific capacitance of the thin-film electrode was unchanged after heating at 160 °C, indicating that the electrochemically active Co sites inside the thin-film electrode were already fully exposed in the as-prepared material. As the heating temperature was raised further, decomposition of the layers of the Co–Al LDHs afforded Co_3O_4, which has good supercapacitor behavior, and $CoAl_2O_4$ which has no electrochemical

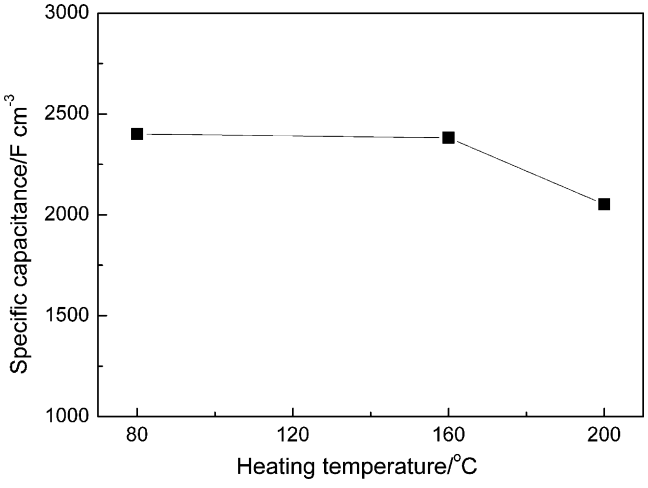

Fig. 11. The specific capacitance of the $Co_{0.80}Al_{0.20}$-LDH NS thin-film electrode as a function of the heating temperature.

activity [35]. This process therefore leads to a decrease in the amount of the active component and an increase in the internal resistance of the thin-film electrode, both of which lead to a deterioration in the supercapacitor behavior of the thin-film electrode.

4. Conclusions

This study shows that continuous $Co_{1-x}Al_x$-LDH NS thin-film electrodes can be fabricated under mild conditions. Varying the Al content x has a significant effect on the electrochemical properties of the thin-film electrode. The partial isomorphous substitution of Co^{2+} by Al^{3+} is the key factor in the improvement of the electrochemical behavior. The $Co_{0.75}Al_{0.25}$-LDH NS thin-film electrode, which has a large specific capacitance of 2500 F cm^{-3} (833 F g^{-1}), a good high-rate capability, and low cost, is an eminently suitable alternative to materials currently used as the electrode for TFSCs. Increasing the thickness of the thin film from 100 to 500 nm has no significant effect on the specific capacitance of the thin-film electrode, which can be attributed to the porous microstructure generated in the original redox reaction and the low internal resistance of the thin-film electrode. Heating the as-deposited thin-film electrode at 160 °C does not give any further enhancement in supercapacitor behaviour. This is due to the fact that the electrochemically active Co sites inside the thin-film electrode already have been fully exposed in the as-prepared Co/Al-LDH NS. This procedure has the potential to be a good route to fabricate high quality thin-film electrodes for micro-scale power sources using electrochemically active inorganic nanosheets.

Acknowledgements

This work was supported by the National Natural Science Foundation of China, the National 863 Project (Grant No. 2006AA03Z343), the 111 Project (Grant No. B07004), and the Program for Changjiang Scholars and Innovative Research Teams in Universities (Grant No. IRT0406).

References

[1] M. Baba, N. Kumagai, H. Kobayashi, O. Nakano, K. Nishidate, Electrochem. Solid-State Lett. 2 (1999) 320–322.
[2] Y.S. Park, S.H. Lee, B.I. Lee, S.K. Joo, Electrochem. Solid-State Lett. 2 (1999) 58–59.
[3] J.B. Bates, N.J. Dudney, B. Neudecker, A. Ueda, C.D. Evans, Solid State Ionics 135 (2000) 33–45.
[4] E.J. Jeon, Y.W. Shin, S.C. Nam, W.I. Cho, Y.S. Yoon, J. Electrochem. Soc. 148 (2001) A318–A322.
[5] H.K. Kim, T.Y. Seong, J.H. Lim, W.I. Cho, Y.S. Yoon, J. Power Sources 102 (2001) 167–171.
[6] J.H. Lim, D.J. Choi, H.K. Kim, W.I. Cho, Y.S. Yoon, J. Electrochem. Soc. 148 (2001) A275–A278.
[7] S.H. Choi, J.S. Kim, Y.S. Yoon, Electrochim. Acta 50 (2004) 547–552.
[8] H.K. Kim, S.H. Choi, Y.S. Yoon, S.Y. Chang, Y.W. Ok, T.Y. Seong, Thin Solid Films 475 (2005) 54–57.
[9] D. Golodnitsky, V. Yufit, M. Nathan, I. Shechtman, T. Ripenbein, E. Strauss, S. Menkin, E. Peled, J. Power Sources 153 (2006) 281–287.
[10] C.L. Li, B. Zhang, Z.W. Fu, J. Electrochem. Soc. 153 (2006) E160–E165.
[11] H. Xia, S.B. Tang, L. Lu, Y.S. Meng, G. Ceder, Electrochim. Acta 52 (2007) 2822–2828.
[12] B.E. Conway, J. Electrochem. Soc. 138 (1991) 1539–1548.
[13] M. Winter, R.J. Brodd, Chem. Rev. 104 (2004) 4245–4269.
[14] S. Sarangapani, B.V. Tilak, C.P. Chen, J. Electrochem. Soc. 143 (1996) 3791–3799.
[15] J.P. Zheng, P.J. Cygan, T.R. Jow, J. Electrochem. Soc. 142 (1995) 2699–2703.
[16] T.R. Jow, J.P. Zheng, J. Electrochem. Soc. 145 (1998) 49–52.
[17] C.C. Hu, W.C. Chen, K.H. Chang, J. Electrochem. Soc. 151 (2004) A281–A290.
[18] C.C. Hu, K.H. Chang, M.C. Lin, Y.T. Wu, Nano Lett. 6 (2006) 2690–2695.
[19] C.C. Hu, K.H. Chang, Electrochim. Acta 45 (2000) 2685–2696.
[20] C.C. Hu, C.Y. Cheng, Electrochem. Solid-State Lett. 5 (2002) A43–A46.
[21] S. Devaraj, N. Munichandraiah, J. Electrochem. Soc. 154 (2007) A80–A88.
[22] K.W. Nam, K.B. Kim, J. Electrochem. Soc. 149 (2002) A346–A354.
[23] L. Cao, M. Lu, H.L. Li, J. Electrochem. Soc. 152 (2005) A871–A875.
[24] S.Y. Wang, K.C. Ho, S.L. Kuo, N.L. Wu, J. Electrochem. Soc. 153 (2006) A75–A80.
[25] Y. Wang, W.S. Yang, J.J. Yang, Electrochem. Solid-State Lett. 10 (2007) A233–A236.
[26] D.G. Evans, X. Duan, Chem. Commun. (2006) 485–496.
[27] Y. Zhao, F. Li, R. Zhang, D.G. Evans, X. Duan, Chem. Mater. 14 (2002) 4286–4291.
[28] J.J. Bravo-Suarez, E.A. Paez-Mozo, S.T. Oyama, Microporous Mesoporous Mater. 67 (2004) 1–17.
[29] L. Cao, F. Xu, Y.Y. Liang, H.L. Li, Adv. Mater. 16 (2004) 1853–1857.
[30] L.Y. Wang, C. Li, M. Liu, D.G. Evans, X. Duan, Chem. Commun. (2007) 123–125.
[31] J.A. Gursky, S.D. Blough, C. Luna, C. Gomez, A.N. Luevano, E.A. Gardner, J. Am. Chem. Soc. 128 (2006) 8376–8377.
[32] D.H. Buss, J. Bauer, W. Diembeck, O. Glemser, J. Chem. Soc., Chem. Commun. (1985) 81–82.
[33] J. Bauer, D.H. Buss, H.J. Harms, O. Glemser, J. Electrochem. Soc. 137 (1990) 173–178.
[34] C. Lin, J.A. Ritter, B.N. Popov, J. Electrochem. Soc. 145 (1998) 4097–4103.
[35] Y. Wang, W.S. Yang, S.C. Zhang, D.G. Evans, X. Duan, J. Electrochem. Soc. 152 (2005) A2130–A2137.